Enhancement of Zener tunneling rate via electron-hole attraction within a time-dependent quasi-Hartree-Fock method

Yasushi Shinohara , Haruki Sanada , and Katsuya Oguri

NTT Basic Research Laboratories, NTT Corporation, 3-1 Morinosato Wakamiya, Atsugi, Kanagawa 243-0198, Japan

The tunneling process, a prototypical phenomenon of nonperturbative dynamics, is a natural consequence of photocarrier generation in materials irradiated by a strong laser. Common treatments for Zener tunneling are based on a one-body problem with a field-free electronic structure. In the literature [Ikemachi *et al.*, Phys. Rev. A **98**, 023415 (2018)], the characteristic of gap shrinking or excitation can occur due to the electron-hole interaction for slow and strong time-varying electric fields. We have developed a theoretical framework called the quasi-Hartree-Fock (qHF) method to enable a more flexible imitation of the electronic structures and electron-hole attraction strength of materials compared with the original Hartree-Fock method. In the qHF framework, the band gap, reduced effective mass, and electron-hole interaction strength can be independently selected to reproduce common crystals. In this paper, we investigate the effect of electron-hole attraction on Zener tunneling subjected to a DC electric field for four different systems using the qHF method. Our findings demonstrate that the electron-hole attraction promotes the tunneling rates in all four material systems assumed as examples. Specifically, systems that have a strong electron-hole interaction show a few factor enhancements for tunneling rates under DC fields, while systems with a weak interaction show higher enhancements of a few tens of percent.

I. INTRODUCTION

Recent progress with strong coherent light source technology has enabled the application of a transient V/nm scale strong field to materials only on the femtosecond time scale. Materials under a strong and short light field exhibit extremely nonlinear responses to the field [1–5] because the field strength is comparable to the electric fields felt by the valence electrons in the materials. Such a strong light field excites photocarriers even in insulators with off-resonant photons, which undergo ablation and permanent damage due to their nonlinear responses [6–8]. When a strong field is applied to vapor, it results in one of the most symbolic phenomena, namely, high-order harmonic generation, in which three steps (field ionization of an electron, electron acceleration by the field, and recombination to the parent ion) govern the mechanism [9]. The number of excited electrons is one of the most important physical quantities of the material exposed to a strong field. According to Keldysh's theory [10], when a strong field makes the tunneling ionization faster than the time scale of the electric field oscillation, i.e., the Keldysh parameter $\gamma < 1$, the optical absorption rate is explained by the ionization due to tunneling rather than that due to multiphoton excitation.

The correlation between the excited electron and the hole corresponds to a local electric field of the same order of magnitude as that of a strong optical pulse. The electron-hole (e-h) interactions are pronounced by the formation of excitons, which play an important role in linear optical absorption processes, especially in systems with low dielectric constants, with low-dimensional structures, and at low temperatures. The research field of two-dimensional materials has progressed

in the past few years [11], where exciton binding energy is at the sub-eV level well above room temperature. Material-dependent excitons are well described by the Bethe-Salpeter equation [12–14] through the dielectric function based on an atomistic quantum mechanical description. The size of the exciton ranges from the subnanometer level to a few nanometers, and its binding energy is from meV to sub-eV. The corresponding field strength can be up to the order of V/nm for tightly bound excitons. While this field strength is comparable to the typical strength of nonlinear optics, the role of exciton existence in nonlinear optical excitation has not yet been investigated.

In rare cases, however, the effects of e-h interaction on the Zener tunneling process [15] have been investigated. The field-induced tunneling property of electrons has been studied mainly in quantum wells [16–18], where theoretical treatments are based on the assumption of rigid energy bands. The Zener tunneling dynamics of atoms in optical lattices also have been investigated mainly within the independent-particle approximation [19–22]. A mean-field treatment of the interatomic potential has been reported [23], but no direct clue was obtained for the e-h effect on the Zener tunneling because the focus was on bosonic systems and contact interaction rather than fermionic systems and long-range interaction. The semiconductor Bloch equation (SBE) [24,25] and time-dependent Hartree-Fock (TD-HF) method are the theoretical frameworks to address the effects of e-h on the Zener tunneling. For example, Garg *et al.* reported the prominent enhancement of photoradiation intensity (i.e., the power spectrum of dipole acceleration) in α-quartz by increasing the e-h interaction strength through SBE simulations [26], where maximally

1.3 eV exciton binding energy is assumed. Ikemachi *et al.* reported a similar enhancement for photoradiation by means of TD-HF calculations for a one-dimensional model [27] in which the exciton binding energy is 3.8 eV. Both investigations did not make an explicit argument for the number of excited electrons, but for photoradiation enhancement by e-h interaction.

Parts of the study by Ikemachi *et al.* [27] indicated that the e-h interaction promotes e-h pair creation, although direct numerical proof was not given. To clarify the background of our current investigation, we briefly review the related part of the study. In their work, the TD-HF method and the *frozen* TD-HF method, where the one-body Hamiltonian is fixed to the initial self-consistent solution, are introduced to calculate high-order harmonic generation for a pulsed electric field. While time-frequency analysis of the frozen TD-HF photoradiation shows good agreement with independent e-h pair motion, the full TD-HF method incorporating e-h interaction shows a higher-frequency emission than the frozen TD-HF method. This higher-frequency component invokes the e-h pair creation promoted by the e-h interaction. While the TD-HF method is the concrete theoretical foundation of the fermionic many-body theory, it is unsuitable for simulating realistic materials' nonperturbative dynamics. A fully converged real-time solution, including a long-range exchange interaction for a given periodic potential, is still limited to spatially one-dimensional systems [27,28] because of the high computational cost. It is hard for the electronic structures and exciton binding energy to imitate common solids (e.g., GaAs and α-quartz) when we utilize the TD-HF framework, especially with one-dimensional space. Therefore most of the TD-HF simulations based on the spatial grid representation have been limited to artificial or quite simple systems such as spatially one-dimensional atomic arrays [27], atoms, or small molecules that contain a few valence electrons.

In light of this background, we have developed a theoretical framework that enables the flexible incorporation of e-h interactions for electron quantum dynamics under a time-dependent external field. The e-h interaction is included at a mean-field level in a quasi-Hartree-Fock (qHF) treatment on top of the electronic structure of an independent electron system (IES). Our qHF provides a simple protocol to obtain a band gap and reduced effective mass values for an IES by choosing a one-body potential. The strength of the e-h interaction is independently selected to reproduce an expected exciton binding energy without affecting the IES in the qHF framework. We perform explicit time evolution of the quantum system under a time-dependent electric field while assuming a DC field as the electric field that induces the tunneling process. This assumption is reasonable when γ is sufficiently smaller than 1, such as the condition ($\gamma = 0.3$ with 2.5 V/nm) discussed in Ikemachi *et al.*'s research [27]. The tunneling rates are estimated from the increasing rate of the number of excited electrons obtained by the time-dependent simulation. We investigate the tunneling rate of electrons under a strong electric field, particularly focusing on the dependence on the electronic structures and the e-h interaction strength.

Section II of this paper presents our theoretical framework. Specifically, we introduce a time-dependent mean-field

theoretical framework for the system consisting of interacting electrons, in which we can flexibly set an arbitrary band gap and an effective mass that determine quasiparticle spectra. In Sec. III, we introduce the details of the simulation protocol, including the complete protocols for numerical simulations and the connection of our tunneling problem. Section IV shows the results of the simulation assuming four different material systems. In Sec. V, we present a discussion, and conclusions are given in Sec. VI. Atomic units are used throughout this paper, where the elementary charge e, electron mass m_e, and Dirac constant $\hbar$ are set to 1.

II. THEORETICAL FRAMEWORK

We derive the equation of motion of the time-dependent quasi-Hartree-Fock (TD-qHF) method from the original TD-HF method. An arbitrary one-body potential can be chosen for the ground state electronic structure within the TD-qHF framework. The potential is determined such that the electronic structure, precisely, the band gap and the reduced effective mass, imitates common materials. The strength of the e-h interaction is independently tuned to give the correct exciton binding energy of the same material. This independent determination of the electronic structure and exciton binding energy is not realized in the original TD-HF framework.

We present the theoretical foundation of the TD-qHF method in terms of three types of properties: (a) The interaction among electrons does not change the electronic ground state as long as the applied field is zero, (b) the energy to be conserved without the applied field can be defined in terms of orbital functions, and (c) there is an explicit orbital set that satisfies the conditions of energy minima. These inspections manifest that our initial wave function is the stable point of the total energy and has almost the same theoretical foundation as the TD-HF method.

A. Time-dependent quasi-Hartree-Fock method

We begin with the spatially one-dimensional TD-HF (1D-TD-HF) equation based on the Born–von Kármán (BvK) boundary condition:

$$i\frac{\partial}{\partial t}\psi_{i,k}(x,t) = \left[\frac{1}{2}\left(-i\frac{\partial}{\partial x} + A(t)\right)^2 + v_{\text{ext}}(x)\right]\psi_{i,k}(x,t)$$
$$+ \hat{v}_{\text{MF}}[\rho]\psi_{i,k}(x,t), \quad (1)$$

$$\hat{v}_{\text{MF}}[\rho]\psi_{i,k}(x,t) = \int_0^{N_k a} dx' \rho(x',x',t)w(x-x')\psi_{i,k}(x,t)$$
$$- \frac{1}{2}\int_0^{N_k a} dx' \rho(x,x',t)w(x-x')\psi_{i,k}(x',t),$$
$$(2)$$

$$\rho(x,x';t) = 2\sum_{i,k}\psi_{i,k}(x,t)\psi_{i,k}^*(x',t), \quad (3)$$

$$\psi_{i,k}(x,t) = \frac{1}{\sqrt{N_k}}e^{ikx}u_{ik}(x,t), \quad (4)$$

where a, v_{ext}, $w(x-x')$, and N_k are the lattice constant, the external potential, the modeled Coulombic interaction between electrons, and the number of primitive cells for the

simulation box. The summation in the density matrix ρ is taken over occupied bands. The number of primitive cells N_k should be as high as possible to obtain well-converged results. The external potential has the lattice periodicity $v_{\text{ext}}(x + a) = v_{\text{ext}}(x)$. The crystal momentum k has the discretized values of $0, 2\pi/(aN_k), 4\pi/(aN_k), \ldots, 2(N_k - 1)\pi/(aN_k)$. The external potential is supposed to be the Coulombic attraction potential from the ion array. The orbital function ψ_k is orthonormalized in the simulation cell as $\int_0^{N_k a} dx\, \psi_{i,k}^*(x, t)\psi_{j,k'}(x, t) = \delta_{i,j}\delta_{k,k'}$, while the lattice periodic part (LPP) u_{ik} is orthonormalized in the unit cell. Here, the spin-restricted wave function for the Slater determinant is assumed, i.e., up- and down-spin orbitals are the same spatial orbital. A k-resolved density matrix is a useful intermediate variable, as

$$\rho^k(x, x'; t) = 2 \sum_i u_{ik}(x, t)u_{ik}^*(x', t), \qquad (5)$$

with $\rho(t) = \frac{1}{N_k} \sum_k e^{ikx} \rho^k(t) e^{-ikx}$.

The mean-field (MF) part (2) in the TD-HF equation has a linear dependence on the density matrix ρ. For an arbitrary density matrix ρ_0, the mean-field part has the following relation:

$$\hat{v}_{\text{MF}}[\rho]\psi_{i,k}(x, t) = \hat{v}_{\text{MF}}[\rho_0]\psi_{i,k}(x, t) + \hat{v}_{\text{MF}}[\rho - \rho_0]\psi_{i,k}(x, t). \qquad (6)$$

Now, we introduce an approximation to the treatment of the Hamiltonian, as

$$\{v_{\text{ext}}(x) + \hat{v}_{\text{MF}}[\rho_0]\}\psi_{i,k}(x, t) \to v(x)\psi_{i,k}(x, t), \qquad (7)$$

$$\rho_0(x, x'; t) = e^{+iA(t)x}\left(2 \sum_{i,k} \phi_{i,k}(x)\phi_{i,k}^*(x')\right)e^{-iA(t)x'}, \qquad (8)$$

$$\left[\frac{1}{2}\left(-i\frac{\partial}{\partial x} + k\right)^2 + v(x)\right]v_{i,k}(x) = \epsilon_{i,k}v_{i,k}(x), \qquad (9)$$

$$\phi_{i,k}(x) = \frac{1}{\sqrt{N_k}}e^{ikx}v_{ik}(x), \qquad (10)$$

$$\psi_{i,k}(x, t = 0) = \phi_{i,k}(x), \qquad (11)$$

where the effective one-body potential is assumed to be the same lattice periodicity $v(x + a) = v(x)$. Note that ρ_0 parametrically depends on the time due to the velocity gauge choice. The mean-field potential at the Hartree-Fock ground state is replaced by the spatially local potential v. We solve the following time-dependent equation of motion rather than the original time-dependent HF equation (1):

$$i\frac{\partial}{\partial t}\psi_{i,k}(x, t) = \left[\frac{1}{2}\left(-i\frac{\partial}{\partial x} + A(t)\right)^2 + v(x)\right]\psi_{i,k}(x, t)$$
$$+ \hat{v}_{\text{MF}}[\rho - \rho_0]\psi_{i,k}(x, t), \qquad (12)$$

called the TD-qHF equation.

The beauty of the TD-qHF equation is that we can reduce it to an equation of motion for the IES by omitting the MF part from Eq. (17). The dynamics of the IES, as determined by the Hamiltonian $[-i\partial/\partial x + A(t)]^2/2 + v(x)$, are regarded as reference dynamics. We can solely change the influence

of the electron-hole interaction on the dynamics by changing the strength of the MF term. We can also prepare an arbitrary potential for v to create an expected electronic structure to simulate different materials, from ideal toy crystals to common crystals. This helpful nature is impossible for the original TD-HF equation because the modeled Coulombic interaction w affects the dynamics as well as the quasiparticle spectra of the reference system.

Here, let us explain the relation between the TD-qHF equation and the famous SBE [24,25]. The TD-qHF equation is equivalent to the SBE when the LPP eigenfunction of $-\frac{1}{2}\frac{\partial^2}{\partial x^2} + v(x)$ does not depend on k and the short-range part of the Coulombic potential is neglected (see Appendix B). TD-qHF is therefore applicable to systems that have tightly bound excitons (e.g., Frenkel exciton). Coulomb matrix elements between pairwise orbitals are more naturally introduced than when using the SBE. Moreover, the TD-qHF method via Eq. (12) is free from the phase determination of the dipole matrix element [29,30] unless the Houston basis is introduced.

A representation of the physical picture embedded in the TD-qHF method is depicted in Fig. 1. All k points of valence (conduction) bands are fully occupied (unoccupied) initially because our system is a band insulator. The off-diagonal component of the density matrix $\rho_{cv} = \langle v, k+A(t)|\rho^k|c, k+A(t)\rangle$ appears when an e-h pair is created. The Landau-Zener (LZ) model provides a good description when only two diabatic components dominate the electronic structure around the gap narrowest point (GNP) ($k = \pi/a$ in this case), as discussed in Sec. III C, where $k + A(t)$ is the time-dependent parameter of the LZ model. Through this process, the population in the conduction (valence) band increases (decreases), as indicated by the solid circle (open circle) in Fig. 1(a). The e-h pairs on different k points are totally independent of the IES by definition. When a dynamic starting from a Γ point is drawn, different k points reveal the same dynamic. This bifurcation process starting from a k point alternately happens in time because an $A(t) \sim -E_{\text{DC}}t$ shape is assumed for the DC field, and the Brillouin zone (BZ) has periodicity in the reciprocal space. By including an e-h interaction, density-matrix components in different k points interact with each other by means of the Coulomb interaction w. When we consider only the long-range part of the Coulomb potential written as w^q, an additional field $-\sum_q w^q \rho_{vc}^{k-q}$ appears in the equation of motion for ρ_{vc}^k, as described by Eq. (B16). Note that the Coulomb potential w in the TD-qHF method couples not only ρ_{vc}^k and ρ_{vc}^{k-q} but also other density-matrix components, as discussed in Sec. III and Appendix B.

B. Theoretical foundation of the TD-qHF method

We need to examine this equation of motion (12) to determine whether or not the expected conditions are satisfied. The first point is to see whether the arbitrary one-body observable $\sum_{ik}\langle\psi_{ik}(t)|\hat{o}|\psi_{ik}(t)\rangle$ is a constant in time without the field. This condition is confirmed by the fact that a trial solution $\tilde{\psi}_{i,k}(x, t) = e^{-i\epsilon_{i,k}t}\phi_{i,k}(x)$ is the solution of Eq. (12) without the field, since $\hat{v}_{\text{MF}}$ vanishes when ρ from the trial solution is equivalent to ρ_0. The solution does not change the observables of any one-body operator. Therefore $\hat{v}_{\text{MF}}$ does not change the
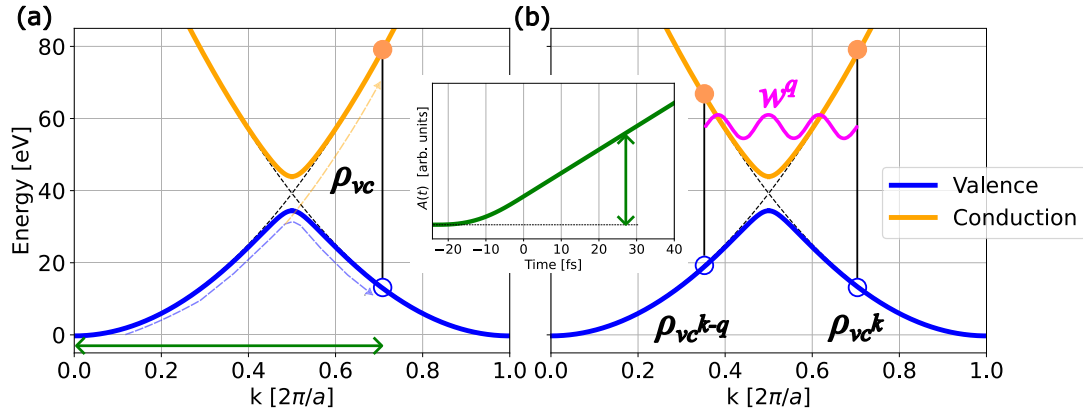
FIG. 1. Schematic image of tunneling ionization for (a) an IES and (b) the TD-qHF method on top of an IES. The band structure for the Hamiltonian of the 1D-TD-HF system as an example is denoted by solid curves. The A-field shape is shown in the inset. Nonadiabatic transition occurs when an orbital in k space passes the narrowest point of the gap due to the intraband motion via the A field, where diabatic levels are drawn as dashed lines.

Slater determinant composed by $\psi_{i,k}$ as long as we set the proper initial condition for ψ_{ik} when the field is absent.

For the second point, we need to see if there is an energy expression as a function of ψ_{ik}. This energy expression should give a constant value for an arbitrary ψ_{ik}, not necessarily $\phi_{i,k}$ under the initial condition, obeying Eq. (12) as long as the external field is zero. A possible energy functional is given as

$$
E[\psi, \psi^*] = 2 \sum_{i,k} \int dx \psi^*_{i,k}(x,t) \left[\frac{1}{2} \left(-i \frac{\partial}{\partial x} + A(t) \right)^2 + v(x) \right] \psi_{i,k}(x,t)
$$
$$
+ \sum_{i,k} \int dx [\psi^*_{i,k}(x,t) \hat{v}_{\mathrm{MF}}[\rho - \rho_0] \psi_{i,k}(x,t) - e^{-iA(t)x} \phi^*_{i,k}(x) \hat{v}_{\mathrm{MF}}[\rho - \rho_0] \phi_{i,k}(x) e^{+iA(t)x}]. \tag{13}
$$

We can show that the equation of motion (12) is obtained as the functional derivative of the energy with respect to the orbital, as

$$
i \frac{\partial}{\partial t} \psi_{i,k}(x,t) = \frac{1}{2} \frac{\delta E}{\delta \psi^*_{i,k}(x,t)},
$$
$$
-i \frac{\partial}{\partial t} \psi^*_{i,k}(x,t) = \frac{1}{2} \frac{\delta E}{\delta \psi_{i,k}(x,t)}, \tag{14}
$$

where half of the prefactor in the energy functional derivative reflects that the total energy is for both spins and the orbital is for each spin. These relations ensure that the energy (13) is conserved in a time-dependent manner as long as the external field A is a constant in time even for orbitals other than the initial one, because of

$$
\frac{d}{dt} E[\psi, \psi^*] = \sum_{i,k} \int dx \left[\frac{\partial \psi^*_{i,k}(x,t)}{\partial t} \frac{\delta E}{\delta \psi^*_{i,k}(x,t)} + \frac{\delta E}{\delta \psi_{i,k}(x,t)} \frac{\partial \psi_{i,k}(x,t)}{\partial t} \right]
$$
$$
+ 2 \frac{dA}{dt} \sum_{i,k} \int dx \psi^*_{i,k}(x,t) \left[-i \frac{\partial}{\partial x} + A(t) \right] \psi_{i,k}(x,t) - \frac{1}{2} \iint dx dx' \frac{\partial \rho_0(x,x';t)}{\partial t} w(x',x) \rho(x',x;t)
$$
$$
= \frac{dA}{dt} \left\langle -i \frac{\partial}{\partial x} + A(t) \right\rangle - \frac{1}{2} \left\langle \frac{\partial \rho_0(t)}{\partial t} w \right\rangle. \tag{15}
$$

Finally, we determine the orbital set that gives the energy minima for the energy functional (13) without the field. The stationary condition of energy with respect to orthonormalized orbitals is given by the condition that $\delta (E - \sum_{nm,k'} \lambda_{nm,k} \langle \tilde{\psi}_{n,k'} | \tilde{\psi}_{m,k'} \rangle) / \delta \tilde{\psi}_{i,k}(x) = 0$, where $\lambda_{nm,k}$ is the Lagrange multiplier to ensure the orthogonality. Using the standard procedure to derive the Hartree-Fock equation, this condition leads to nonlinear eigenvalue equations, as

$$
\tilde{\epsilon}_{i,k} \tilde{\psi}_{i,k}(x) = \left[-\frac{1}{2} \frac{\partial^2}{\partial x^2} + v(x) + \hat{v}_{\mathrm{MF}}[\tilde{\rho} - \rho_0] \right] \tilde{\psi}_{i,k}(x),
$$
$$
\tilde{\rho}(x,x') = 2 \sum_{i,k} \tilde{\psi}_{i,k}(x) \tilde{\psi}^*_{i,k}(x'). \tag{16}
$$

In general, the eigenvector ψ_{ik} should be determined in the self-consistent field manner, as in the original Hartree-Fock equation. Here, a trivial solution of Eq. (16) is achieved by $\tilde{\psi}_{i,k} = \phi_{i,k}$, $\tilde{\rho} = \rho_0$, and $\tilde{\epsilon}_{i,k} = \epsilon_{i,k}$. Therefore the initial condition of the TD-qHF equation $\phi_{i,k}$ gives a variationally stationary value of the energy functional (13).

III. SIMULATION SCHEME

We introduce an explicit discretization scheme for the spatial coordinate to solve Eq. (12). The LPP is expressed as the sum of plane waves that have reciprocal lattice momenta. Whole ingredients in the equation of motion are written as matrix elements evaluated as the reciprocal lattice momentum. A predictor-corrector trick in time propagation is needed to obtain a reasonable solution when the e-h interaction is switched on.

Then, we derive an explicit formula to determine the one-body potential. The band gap and the reduced effective mass are analytically determined by the potential amplitude and the lattice constant within the degenerated perturbation theory among two energy branches [31]. The time-dependent problem of the two-band assumption results in mapping to the Landau-Zener-type (LZ-type) Hamiltonian when we neglect the e-h interaction.

We extract the tunneling rates from a real-time solution of the TD-qHF equation. We solve the time-dependent equation of motion under a time-dependent field where the electric field is kept constant after a slow ramp-up field. The number of excited electrons (NEE) is evaluated by the explicit projection of the time-dependent wave function onto conduction bands. The tunneling rate is obtained as the slope of the NEE as a function of time, which is validated as long as the slope is constant in time. Compared with a stationary assumption to obtain the rate, where different assumptions lead to different values [21], this tunneling rate evaluation is the most direct and concrete way to obtain the tunneling rate for a given system.

A. Discretization for numerical simulation

We here derive the exact expression of the LPP function in the TD-qHF method. We utilize plane wave expansion for the LPP, as $u_{i,k}(x, t) = \sum_G e^{iGx} u_{i,k}(G, t)$, with $G = 2\pi n/a$ and $n = 0, \pm 1, \pm 2, \ldots$. The equation of motion for the LPP is given as

$$i\frac{d}{dt}u_{i,k}(G, t) = \frac{1}{2}([G + k + A(t)]^2 u_{i,k}(G, t)$$
$$+ \sum_{G'} v_{G-G'} u_{i,k}(G', t) + \sum_{G'} v_{MF,G,G'}^k[\rho - \rho_0]$$
$$\times u_{i,k}(G', t), \qquad (17)$$

$$v_{MF,G,G'}^k[\varrho(t)] = N_k a w^{q=0}(G - G')\eta(G - G', t)$$
$$- \frac{N_k a}{2} \sum_{q,H} w^q(H)\varrho^{k-q}(G - H, G' - H; t), \qquad (18)$$

where the relevant Fourier components are given as

$$w^k(G) = \frac{1}{N_k a}\int_0^{N_k a} dx\, e^{-i(k+G)x} w(x), \qquad (19)$$

$$v_G = \frac{1}{a}\int_0^a dx\, e^{-iGx} v(x), \qquad (20)$$

$$\eta(G, t) = \frac{1}{a}\int_0^a dx\, e^{-iGx}\varrho(x, x; t), \qquad (21)$$

$$\rho^k(G, G'; t) = 2\sum_i u_{ik}(G, t)u_{ik}^*(G', t), \qquad (22)$$

$$\rho_0^k(G, G'; t) \simeq 2\sum_i v_{i,k+A(t)}(G)v_{i,k+A(t)}^*(G'). \qquad (23)$$

The approximately equal sign in the last formula comes from the following approximation:

$$\frac{1}{N_k a}\int_0^{N_k a} dx\, e^{i\kappa x} = \frac{1}{iN_k a\alpha}(e^{i\kappa N_k a} - 1) \xrightarrow{N_k a \to \infty} \delta_{\kappa, 0}. \qquad (24)$$

The spatial integration (24) becomes exact when κ is on a k grid. Thus the large-N_k limit ensures that this approximation becomes accurate because we can find any $k + A(t)$ from the infinitely dense k grids. The finite spatial integration for $w^k(G)$ leads to a spatial periodicity of the real-space counterpart: $w_{N_k}(x) = \sum_{k,G} w^k(G)e^{i(k+G)x}$, $w_{N_k}(x + N_k a) = w_{N_k}(x)$. The real-space counterpart $w_{N_k}(x)$ becomes the original $w(x)$ when we take a large-N_k limit. The reciprocal grids for G and k are dense enough to obtain well-converged results. The shifted eigenvector $v_{i,k+A(t)}(G)$ is constructed by explicit diagonalization each time step from the time-dependent Hamiltonian, $\frac{1}{2}[G + k + A(t)]^2\delta_{G,G'} + v_{G-G'}$.

B. Time-evolution protocol

We utilize a unitary matrix as the propagator of the orbital function, as

$$u_{i,k}(G, t + \Delta t) = \sum_{G'} U_{G,G'}(h^k)u_{i,k}(G', t), \qquad (25)$$

$$U_{G,G'}(h_k) = \left\langle G\left|\sum_n e^{-ih_k\Delta t}\right|G'\right\rangle, \qquad (26)$$

where h^k is a k-dependent Hermitian matrix (similar to the Hamiltonian). The unitary matrix is obtained from an explicit diagonalization of h^k. The unitary nature guarantees norm conservation in the time propagation regardless of h^k choice.

We utilize a predictor-corrector (PC) scheme for the selection of h^k [32]:

$$h^k = \frac{1}{2}\{h_{qHF}^k[\rho(t)](t) + h_{qHF}^k[\rho^p](t + \Delta t)\}, \qquad (27)$$

$$h_{qHF}^k[\varrho](t) = \frac{1}{2}[G + k + A(t)]^2\delta_{G,G'}$$
$$+ v_{G-G'} + v_{MF,G,G'}^k[\varrho - \rho_0], \qquad (28)$$

where ρ_0 is constructed with $A(t)$. ρ^p is the predictor constructed by

$$u_{i,k}^p(G) = \sum_{G'} U_{G,G'}(h_{qHF}^k[\rho(t)](t))u_{i,k}(G', t),$$

$$\rho^p = \frac{2}{N_k}\sum_i e^{+ikx}u_{i,k}^p(x)u_{i,k}^{p*}(x')e^{-ikx'}. \qquad (29)$$

Thus we need to perform unitary matrix construction and the matrix-vector operation twice to move one step forward.

This PC scheme for the unitary matrix construction is mandatory for the qHF case, namely, the case with the electron-hole interaction. Results without a PC lead to unphysical behavior even for a short time step $\Delta t = 0.02$ a.u. = 0.484 as when a large α is used in Eq. (39), although unitarity in the time propagation is guaranteed by the construction. We confirm that $\Delta t = 0.2$ is usually small enough for our systems when we use the PC scheme.

C. Band gap, reduced mass, and tunneling rate within the Landau-Zener model for a monochromatic potential

We explain the protocol to obtain an arbitrary band gap and reduced mass for the e-h pair derived from a one-body potential v. We utilize the monochromatic spatial potential, having only one wave number, to give an expected gap and mass. The reference dynamics can be approximately mapped to the Landau-Zener (LZ) model in the monochromatic potential. The LZ model is utilized to provide our reference system with a tunneling rate estimation. We concentrate on an IES throughout this section.

To keep our problem as simple as possible, we consider a system that has only one band gap in the BZ within the degenerated perturbation theory. Specifically, we choose fully occupied (unoccupied) states below (above) the gap and investigate the transition from the occupied valence band to the unoccupied conduction band. The single gap is achieved by the potential $v(x) = v_0 \cos(2\pi n \frac{x}{a})$, $n = 1, 2, \ldots$. The Fourier transformation is given as

$$v_{G-G'} = v_0(\delta_{G-G', n2\pi/a} + \delta_{G-G', -n2\pi/a}). \tag{30}$$

This potential connects three components $(G, G'_\pm = G \pm n2\pi/a)$ in Eq. (17) when the mean field is neglected. The kinetic energy for the G and $G'_\pm$ components degenerates at $k_\pm = -G \mp n\pi/a$. Another kinetic energy for the $G'_\mp$ component $\frac{9}{2}(n\pi/a)^2$ is far from the degenerated energy $\frac{1}{2}(n\pi/a)^2$. Hereinafter, we denote G' as either G'_+ or G'_-. Therefore a 2×2 matrix representation for the time-dependent Schrödinger equation is justified by

$$i\frac{d}{dt}\begin{pmatrix} u_k(G, t) \\ u_k(G', t) \end{pmatrix} = \begin{pmatrix} \frac{1}{2}[G + k + A(t)]^2 & v_{G-G'} \\ (v_{G-G'})^* & \frac{1}{2}[G' + k + A(t)]^2 \end{pmatrix} \begin{pmatrix} u_k(G, t) \\ u_k(G', t) \end{pmatrix}. \tag{31}$$

In the degenerate perturbation theory among two levels [31], the band gap Δ appears in accordance with the amount of $2|v_{G-G'_\pm}|$ at $k = -\frac{G+G'_\pm}{2}$. To get rid of the k-squared term in the Hamiltonian, we introduce a time-dependent phase factor associated with the average energy $\frac{1}{4}\{[G + k + A(t)]^2 + [G' + k + A(t)]^2\}$ as $(\tilde{u}_\kappa^G(t), \tilde{u}_\kappa^{G'}(t))^T = e^{-i\frac{1}{4}\{[G+k+A(t)]^2+[G'+k+A(t)]^2\}} \times (u_\kappa^G(t), u_\kappa^{G'}(t))^T$, with a variable change $\kappa = k + \frac{G+G'}{2}$.

$$i\frac{d}{dt}\begin{pmatrix} \tilde{u}_\kappa(G, t) \\ \tilde{u}_\kappa(G', t) \end{pmatrix} = \begin{pmatrix} \frac{1}{2}(G - G')[\kappa + A(t)] & v_{G-G'} \\ (v_{G-G'})^* & -\frac{1}{2}(G - G')[\kappa + A(t)] \end{pmatrix} \begin{pmatrix} \tilde{u}_\kappa(G, t) \\ \tilde{u}_\kappa(G', t) \end{pmatrix}. \tag{32}$$

The shifted crystal momentum κ means a crystal momentum measured from the degenerated point.

The DC electric field is obtained by $A(t) = -E_{DC}t$. By choosing a proper time origin, the crystal momentum κ can be set to zero. Thus Eq. (32) can be exactly mapped to the LZ model [33]. The adiabaticity parameter given in Ref. [21] is $\varepsilon = (G - G')E_{DC}/(2|v^{G-G'}|^2)$.

Let us derive formulas for the effective mass (32) written as $v_{G-G'}$ and $G - G'$. By diagonalizing the Hamiltonian in (32) with $A = 0$, we have two energy branches:

$$\epsilon_\pm(\kappa) = \pm\sqrt{\frac{1}{4}(G - G')^2\kappa^2 + |v_{G-G'}|^2}. \tag{33}$$

Regarding $+$ and $-$ as conduction and valence bands, the reduced effective mass μ reads

$$\frac{1}{\mu} = \left(\frac{d^2\epsilon_+}{d\kappa^2}\right)_{\kappa=0}^{-1} - \left(\frac{d^2\epsilon_-}{d\kappa^2}\right)_{\kappa=0}^{-1} = \frac{(G - G')^2}{\Delta}, \tag{34}$$

where $\Delta = 2|v_{G-G'}|$. The pure imaginary momentum that gives zero eigenvalues of the Hamiltonian in (32) is $\kappa = i\sqrt{\mu\Delta}$. The diabatic transition amount for $t = -\infty$ to ∞ is given as $e^{-\pi/\varepsilon}$ [21], with $1/\varepsilon = \sqrt{\mu\Delta}\Delta/(2E_{DC})$. This amount is the incremental value in the event that the vector potential

sweep crosses $A(t) = 0$. This transition alternatively happens in crystals because the vector potential sweeps over Brillouin zones with the constant velocity E_{DC} (see Fig. 1). The period of the event is $2\pi/(aE_{DC})$, as this is how long it takes to pass the first Brillouin zone once for the vector potential. Then, we obtain the tunneling rate as

$$w_{LZ} = \frac{aE_{DC}}{2\pi}e^{-\pi\sqrt{\mu\Delta}\Delta/(2E_{DC})}. \tag{35}$$

The exponential dependence is the same as the semiclassical treatment of the Zener tunneling [34]. This LZ treatment does not include a resonance tunneling structure as a function of E_{DC} because there is no $1/E_{DC}$ oscillation in (35). To obtain a more qualitative rate, a finite time interval rather than $-\infty$ to ∞ should be taken into account for the LZ transition amount [21]. The finite interval $\tau_\pm$ in the normalized LZ formula in Eq. (61) of Ref. [21] for $|G - G'| = n\frac{2\pi}{a}$ is given as

$$\tau_\pm = \pm\frac{1}{2n\mu}, \tag{36}$$

where we use the normalized time $\tau/t = |G - G'|E_{DC}/(2|v_{G-G'}|) = E_{DC}/(\sqrt{\mu\Delta})$. Thus, having a smaller n

and lighter μ leads to a better approximation of Eq. (35) to Zener tunneling.

While an interpretation of the Keldysh parameter combined with the LZ treatment provides interesting insights, it does not relate to our problem directly. This consideration is given in more detail in Appendix A.

The tunneling formula (35) itself is for pairwise states and is not intended to rely on the spatial dimension of reciprocal space. In other words, the tunneling rate can be a fair value for systems that have different spatial dimensions. The Brillouin zone integration is required to obtain the actual number of excited electrons for pairwise states per length, surface, or volume. We further need the factor 2 because of spin degeneracy.

We need to determine how many electrons are in the primitive cell. We assume a band insulator where the bottom N_{occ} bands are occupied for the initial condition in the reference system. The electron number per cell is $2N_{occ}$ because of the spin degeneracy. Our potential $v(x) = v_0 \cos(2\pi nx/a)$ gives a gap $2v_0$ between the nth and $(n+1)$th bands according to the degenerated perturbation theory. Since we focus on Zener tunneling from valence top to conduction bottom, we set $n = N_{occ}$.

D. Tunneling rate evaluation from real-time calculation

We apply a DC electric field after a smooth ramp-up to get rid of excitations due to the sudden field switch-on. The actual field shape is

$$A(t) = \begin{cases} -E_{DC}T\left[\frac{(t+T)^3}{T^3} - \frac{(t+T)^4}{2T^4}\right] & (-T \leqslant t < 0) \\ -E_{DC}(t + T/2) & (0 \leqslant t), \end{cases} \quad (37)$$

as shown in the inset in Fig. 1. The electric field is obtained as the temporal derivative by $E(t) = -\dot{A}$. In the ramp-up region, the electric field exhibits a cubic function, $E_{DC}[3(t + T)^2/T^2 - 2(t + T)^3/T^3]$ $(-T \leqslant t < 0)$, for connecting smoothly to the constant value. The field shape gives $\dot{E}(-T) = \dot{E}(0) = 0$. We take $T = 1000 = 24.19$ fs $= \hbar/(0.171 \text{ eV})$ for the simulations over all parameters. The energetic dimension, 0.171 eV, is much less than the band gaps of the four investigated systems.

We define the NEE as

$$N_{ex}(t) = \frac{2}{N_k} \sum_{i,b(\in \text{unocc}),k} \int_0^a dx \, v_{b,k+A(t)}^*(x) u_{i,k}(x,t), \quad (38)$$

where the instantaneous eigenfunction $v_{b,k+A(t)}$ is obtained by an explicit diagonalization each time. For oscillating electric fields, projection onto the instantaneous eigenfunctions is more suitable for evaluating the NEE under finite electric fields [35] than field-free eigenfunctions. The NEE is normalized in a unit cell, i.e., it is equal to the total number of electrons in the cell when all electrons are excited from valence bands. To obtain the excited carrier density, we need to multiply the cell volume, area, or length by the NEE.

We fit the slope value as the tunneling rate for the temporal evolution of the NEE from a real-time solution of the TD-qHF equation. The LZ transition happens once in a period $T_B = 2\pi/(aE_{DC})$, which is the period of the Bloch oscillation. The tunneling rate is not expected to be stationary for $0 \leqslant t < T_B$ because the LZ transition occurs only once. The fitting is

TABLE I. Data set and physical constants derived from the Wannier equation for the four systems. The number of occupied bands N_{occ} is always 1. a, v, Δ, and E_{op} are in atomic units.

System	a (a.u.)	v (a.u.)	α	μ	Δ (a.u.)	E_{op} (a.u.)	Ref.
(a) 1D-TD-HF	1.85	0.174	0.68	0.0303	0.3487	0.2105	[27]
(b) BN sheet	7.05	0.143	0.21	0.360	0.2860	0.2131	[36]
(c) α-quartz	6.4	0.167	0.059	0.347	0.3340	0.3219	[37]
(d) GaAs	5.0	0.028	0.01	0.0355	0.05600	0.05591	[38]

performed for the slope after T_B. As shown in the figures in Sec. IV, most of the data show a nicely linear dependence on time for the regime.

IV. RESULTS

We prepare four systems imitating (a) a one-dimensional time-dependent Hartree-Fock (1D-TD-HF) solution [27], (b) a boron-nitride sheet (BN sheet), (c) α-quartz, and (d) GaAs. The characteristics of the systems are (a) extreme conditions for electron-hole attraction strength, (b) a two-dimensional semiconductor, (c) a three-dimensional insulator, and (d) a three-dimensional semiconductor. Note that these simulations only utilize one-dimensional integration over the Brillouin zone. These different materials are imitated using only the band gap, effective mass, and exciton binding energy, as described in the following sections. The effective Coulomb interaction is expected to capture the main role of e-h interaction for the tunneling dynamics. The remaining effect (e.g., dynamical symmetry) is missing within the one-dimensional treatment.

We change the reciprocal lattice size $2\pi/a$, the number of occupied bands N_{occ}, and the off-diagonal component $v_{G-G'}$ to obtain the given band gaps and effective masses of the reference systems. The number of occupied bands is set to 1 for simplicity. We utilize a scaled electron-electron interaction, as

$$w(x) = \frac{\alpha}{\sqrt{1 + x^2}}. \quad (39)$$

The softened Coulomb potential has a long-range tail and no singularity at the origin. The strength α is chosen such that the one-dimensional Wannier equation (B22) gives exciton binding energies that correspond to reported values; see Appendix B for more details. Here, E_{op} is introduced as the optical gap from the Wannier equation. The exciton binding energy is obtained as $E_{op} - \Delta$. We utilized parameters a, v, and α (Table I) and confirmed that they give μ, Δ, and E_{op} in a large enough Brillouin zone sampling for static calculation.

A. 1D-TD-HF system

The first system imitates the time-dependent Hartree-Fock results reported in Ref. [27]. This system is more or less artificial due to the one-dimensional space treatment with the TD-HF method, leading to a strong electron-hole attraction. However, the strong effect provides insight into how the electron-hole interaction affects the dynamics. The band gap and the reduced effective mass for quasiparticle spectra are $\Delta = 0.35 = 9.5$ eV and $\mu = 0.03$, as obtained by the
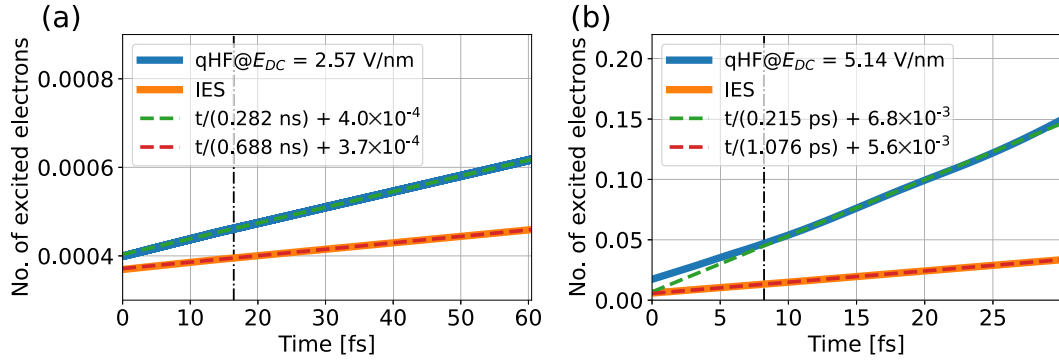
FIG. 2. Number of excited electrons as a function of time for a 1D-TD-HF system under (a) $E_{DC} = 2.6$ V/nm and (b) $E_{DC} = 5.1$ V/nm. The T_B values of 16.52 and 8.26 fs are represented as vertical dash-dotted lines in (a) and (b), respectively.

self-consistent Hartree-Fock solution in Ref. [27]. The exciton binding energy is 3.8 eV obtained through the linear response spectra derived from the direct real-time solution of the TD-HF method. The normalized time interval (36) is given as $\tau_\pm = \pm 16.5$.

First, we fix the off-diagonal component $v = 0.174$ to reproduce the band gap. Then, the lattice constant is set to $a = 1.85$ to reproduce the reduced effective mass. Finally, the strength of the electron-electron interaction is determined as $\alpha = 0.68$ by a condition such that the Wannier equation (B22) gives the same binding energy as the TD-HF result in Ref. [27].

We use 13 and 400 grids for real and reciprocal space, respectively, to obtain well-converged results. The size of the time step is $0.02 = 0.484$ as, which is quite a small value and only mandatory with e-h interaction. The IES dynamics require $0.2 = 4.84$ as for the time step.

The time evolution of the NEE for the DC field is presented in Fig. 2, where both graphs show linear behavior as a function of time after T_B. There are finite y intercepts because the ramp-up field influences the dynamics for $t < 0$. By linear fitting with $wt + n$ for $0.005 = 2.57$ V/nm excitation, the tunneling rates w for the TD-qHF method and the IES are $8.58 \times 10^{-8} = 1/(0.282$ ns) and $3.52 \times 10^{-8} = 1/(0.688$ ns). The TD-qHF method shows a 2.44 times more significant tunneling rate than the IES. For $0.01 = 5.14$ V/nm excitation, the tunneling rates are $1.12 \times 10^{-4} = 1/(0.215$ ps) and $2.25 \times 10^{-5} = 1/(1.076$ ps), and thus the enhancement factor is 4.98. The tunneling rates and the field-dependent enhancements are summarized in Table II. The LZ formula (35) gives a quantitatively accurate estimation for the IES, which can be attributed to the light-reduced mass.

The NEE is a normalized number in a cell. When the field is 2.57 V/nm, the NEE reaches 0.1% of the total electrons after 1 ps, where two electrons are in the cell. After doubling the strength to 5.14 V/nm, the NEE reaches 0.1% after 1 fs. The abrupt increase in the NEE with respect to the field increase stems from the strong nonlinearity in the tunneling process.

B. BN sheet

The second system imitates a BN sheet, which is a two-dimensional semiconductor. The protocol to determine v, a, and α as the material parameters is the same as for the 1D-TD-HF system. According to Ref. [36], $\Delta = 0.2860 = 7.77$ eV and $\mu = 0.36$ derived from the effective masses for a hole, $m_h = 0.63$, and a particle, $m_e = 0.83$. The binding energy of excitons is 2.14 eV. Then, we utilize the following parameters for the BN sheet: $v = 0.143$, $a = 7.05$, and $\alpha = 0.21$. The normalized time interval (36) is given as $\tau_\pm = \pm 1.39$.

We use 53 and 140 grids for real and reciprocal space, respectively, to obtain well-converged results. The time-step size is 0.2, the same as the IES of the 1D-TD-HF system.

Figure 3 shows the time-dependent NEE values for the BN-sheet system. The tunneling rates are obtained by the same procedure as for the 1D-TD-HF system. For 4.1 V/nm excitation, the tunneling rates are $1.35 \times 10^{-10} = 1/(17.9$ ns) and $4.19 \times 10^{-9} = 1/(57.7$ ns), and thus the enhancement factor is 3.22. The tunneling rates are $5.05 \times 10^{-5} = 1/(479$ fs) and $2.12 \times 10^{-5} = 1/(1140$ fs) for 10.3 V/nm excitation. Table III summarizes the tunneling rates and field-dependent

TABLE II. Calculated tunneling rates and enhancement factors for the 1D-TD-HF system. The period of Bloch oscillation and the tunneling rates evaluated with the LZ formula (35) are tabulated.

E_{DC} (a.u.)	T_B (a.u.)	$2w_{LZ}$ (a.u.)	IES (a.u.)	qHF (a.u.)	Enhancement
0.003	1130	1.25×10^{-11}	1.16×10^{-11}	2.29×10^{-11}	1.97
0.005	680	3.79×10^{-8}	3.52×10^{-8}	8.58×10^{-8}	2.44
0.01	340	2.11×10^{-5}	2.25×10^{-5}	1.12×10^{-4}	4.98

TABLE III. Calculated tunneling rates and enhancement factors for the BN-sheet system. The period of Bloch oscillation and the tunneling rates evaluated with the LZ formula (35) are tabulated.

E_{DC} (a.u.)	T_B (a.u.)	$2w_{LZ}$ (a.u.)	IES (a.u.)	qHF (a.u.)	Enhancement
0.008	111	2.68×10^{-10}	4.19×10^{-10}	1.35×10^{-9}	3.22
0.009	99.0	2.23×10^{-9}	1.47×10^{-9}	2.84×10^{-9}	1.93
0.01	89.1	1.23×10^{-8}	2.84×10^{-7}	1.41×10^{-7a}	0.496[a]
0.015	59.4	2.26×10^{-6}	2.16×10^{-6}	6.44×10^{-6}	2.98
0.02	44.6	3.33×10^{-5}	2.12×10^{-5}	5.05×10^{-5}	2.38

[a]The corresponding NEE does not show a strict linear line.
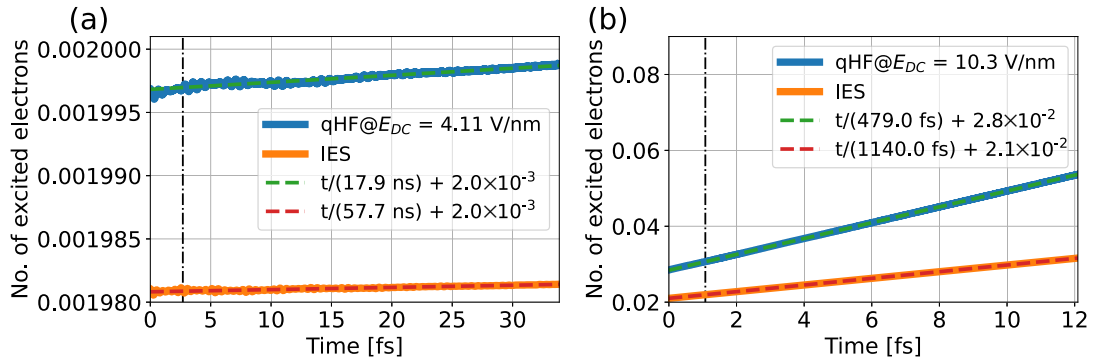
FIG. 3. Number of excited electrons as a function of time for a BN sheet under (a) $E_{DC} = 4.1$ V/nm and (b) $E_{DC} = 10.3$ V/nm. The T_B values of 2.70 and 1.078 fs are represented as dash-dotted vertical lines in (a) and (b), respectively.

enhancements. The ionization rate of qHF with the $E_{DC} = 0.01$ field has significant ambiguity because the NEE does not show a strict linear dependence on time.

Compared with the 1D-TD-HF system, the BN system is barely excited for both the IES and the qHF method, while the band gap is smaller. This is due to the much heavier reduced mass than for the 1D-TD-HF system. Because of this heavier mass, the LZ formula occasionally fails to predict the ionization rate, in contrast to the 1D-TD-HF system. When we assume that the field comes from an optical field, the field intensity for 10.3 V/nm is 14 TW/cm^2. According to a rough estimation that just a half period of a single oscillation effectively ionizes the electron into the conduction band by the tunneling rate, 1% of the photocarriers are generated in 7.5 fs with 14 TW/cm^2 intensity.

C. α-quartz

The third system imitates α-quartz, a three-dimensional insulator. The protocol to determine v, a, and α as the material parameters is the same as before. According to Ref. [37], $\Delta = 0.334 = 9.1$ eV and $\mu = 0.347$ derived from the effective masses for a hole, $m_h = 1.3$, and a particle, $m_e = 0.5$. The binding energy of excitons is estimated to be 0.33 eV, for the hydrogen $1s$ state energy with the screened Coulombic interaction with dielectric constant $\epsilon_r \sim 3.8$ for the reduced mass, and is calculated by $E_n = -\frac{\mu}{2\epsilon_r^2}$. Then, we utilize the following

parameters for α-quartz: $v = 0.167$, $a = 6.4$, and $\alpha = 0.059$. The normalized time interval (36) is given as $\tau_{\pm} = \pm 1.44$.

We use 103 and 40 grids for real and reciprocal space, respectively, to obtain well-converged results. The time-step size is 0.2 a.u., the same as the BN sheet.

Figure 4 shows time-dependent NEE values for the α-quartz system. We used the same procedure for obtaining the tunneling rates as for the 1D-TD-HF system. For $0.02 = 10.3$ V/nm excitation, the tunneling rates are $8.77 \times 10^{-6} = 1/(2.76 \text{ ps})$ and $6.58 \times 10^{-6} = 1/(3.67 \text{ ps})$, and thus the enhancement factor is 1.33. The tunneling rates are $4.86 \times 10^{-4} = 1/(49.7 \text{ fs})$ and $3.24 \times 10^{-4} = 1/(74.7 \text{ fs})$ for $0.03 = 15.4$ V/nm excitation. Table IV summarizes the tunneling rates and field-dependent enhancements.

The tendency of the α-quartz system is similar to that of the BN-sheet system, with a relatively heavy mass and relatively high band gap. One of the most significant differences is the much smaller e-h interaction, mainly due to the high dimensionality. The enhancement of the e-h interaction is in the range of a 16–50% increase in the investigated strength.

D. GaAs

The final system imitates GaAs, a three-dimensional semiconductor. The protocol to determine v, a, and α as the material parameters is the same. According to Ref. [38], $\Delta = 1.519$ eV and $\mu = 0.0377$ derived from the effective masses

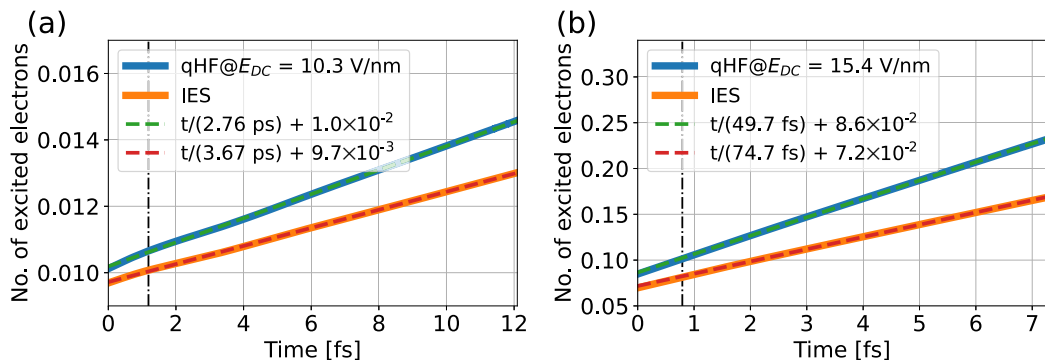FIG. 4. Number of excited electrons as a function of time for α-quartz under (a) $E_{DC} = 10.3$ V/nm and (b) $E_{DC} = 15.4$ V/nm. The T_B values of 1.187 and 0.792 fs are represented as dash-dotted vertical lines in (a) and (b), respectively.

TABLE IV. Calculated tunneling rates and α-quartz system enhancement factors. The period of Bloch oscillation and the tunneling rates evaluated with the LZ formula (35) are tabulated.

E_{DC} (a.u.)	T_B (a.u.)	$2w_{LZ}$ (a.u.)	IES (a.u.)	qHF (a.u.)	Enhancement
0.01	98.2	3.57×10^{-10}	2.59×10^{-10}	3.00×10^{-10}	1.16
0.02	49.1	5.39×10^{-6}	6.58×10^{-6}	8.77×10^{-6}	1.33
0.03	32.7	1.59×10^{-4}	3.24×10^{-4}	4.86×10^{-4}	1.50

TABLE V. Calculated tunneling rates and enhancement factors for the GaAs system. The period of Bloch oscillation and the tunneling rates evaluated with the LZ formula (35) are tabulated.

E_{DC} (a.u.)	T_B (a.u.)	$2w_{LZ}$ (a.u.)	IES (a.u.)	qHF (a.u.)	Enhancement
0.0005	2510	3.12×10^{-7}	3.62×10^{-7}	3.64×10^{-7}	1.01
0.0008	1570	9.46×10^{-6}	8.52×10^{-6}	8.73×10^{-6}	1.02
0.001	1260	3.15×10^{-5}	2.76×10^{-5}	2.93×10^{-5}	1.06

for a light hole, $m_h = 0.087$, and a particle, $m_e = 0.0665$. The binding energy of excitons is estimated to be 0.003 eV for the 1s state energy with a dielectric constant of $\sim$13 for the reduced mass. Then, we utilize the following parameters for GaAs: $v = 0.028$, $a = 5.0$, and $\alpha = 0.01$. The normalized time interval (36) is given as $\tau_\pm = \pm 14.1$.

We use 13 and 140 grids for real and reciprocal space, respectively, to obtain well-converged results. The time-step size is 0.2 a.u., the same as the BN sheet and α-quartz.

Figure 5 shows the time-dependent NEE values for the GaAs system. We used the same procedure to obtain the tunneling rates as for the 1D-TD-HF system. For $0.0008 = 0.411$ V/nm excitation, the tunneling rates are $8.73 \times 10^{-6} = 1/(2.77 \text{ ps})$ and $8.52 \times 10^{-6} = 1/(2.84 \text{ ps})$, and thus the enhancement factor is 1.02. The tunneling rates are $2.93 \times 10^{-5} = 1/(826 \text{ fs})$ and $2.76 \times 10^{-5} = 1/(877 \text{ fs})$ for $0.001 = 0.514$ V/nm excitation. Table V summarizes the tunneling rates and field-dependent enhancements. The LZ formula (35) gives a good estimation for the IES because of the light-reduced mass of GaAs.

The NEE of the GaAs system reached a few electrons in a cell with a much weaker field than the other three systems. This is because GaAs has a light-reduced mass and a much smaller gap. Similar tunneling rates are achieved with a field strength tens of times weaker than that of the α-quartz system. Reflecting the weaker e-h interaction strength, the enhancement due to e-h interaction is minor, up to 0.514 V/nm.

V. DISCUSSION

We examine the trend of the enhancement due to e-h interaction and the tunneling rate over the investigated materials and field, as shown in Fig. 6. The enhancement factors in Fig. 6(a) are normally larger than unity except for the BN-sheet system at $0.01 = 5.14$V/nm, at which ionization rates are not rigorously defined because the NEE does not show a clear straight line. We find a tendency that significant enhancements are accompanied by a large e-h interaction strength α. The enhancement factors increase with field strength increasing for the 1D-TD-HF, α-quartz, and GaAs systems.

The LZ formula basically gives us a reasonable estimation of the tunneling rates for all examples in Fig. 6(b). Specifically, it shows quite a good estimation for the IES when the reduced mass is light, as in the 1D-TD-HF and GaAs systems. For the BN-sheet system, the LZ formula maximally predicts an order error for a heavier mass of around 0.35. The e-h enhancement increases for a stronger field with the 1D-TD-HF, α-quartz, and GaAs systems.

Here, we discuss the mechanism underlying the enhancement due to e-h interaction. Band-gap renormalization (BGR) can be explained as occurring through carrier introduction by photodoping, thermal excitation, or chemical doping. These gap reductions can be explained as the exchange interaction weakening by Eq. (B19) in the two-band SBE. Thus the possible mechanism for enhancing tunneling rates is attributed to electronic structure renormalization. To confirm this mechanism, we perform on-the-fly electronic structure extraction from the time-dependent qHF Hamiltonian $h^k[\rho(t)](t)$. A system that has light effective mass is suitable to evaluate the tunneling rate using the LZ formula. We analyze the data for the 1D-TD-HF system because of its light mass and strong e-h interaction strength.

We evaluate a time-dependent eigenvalue $\mathcal{E}_i^k(t)$ by the explicit diagonalization of $h^k[\rho(t)](t)$, where i refers to the
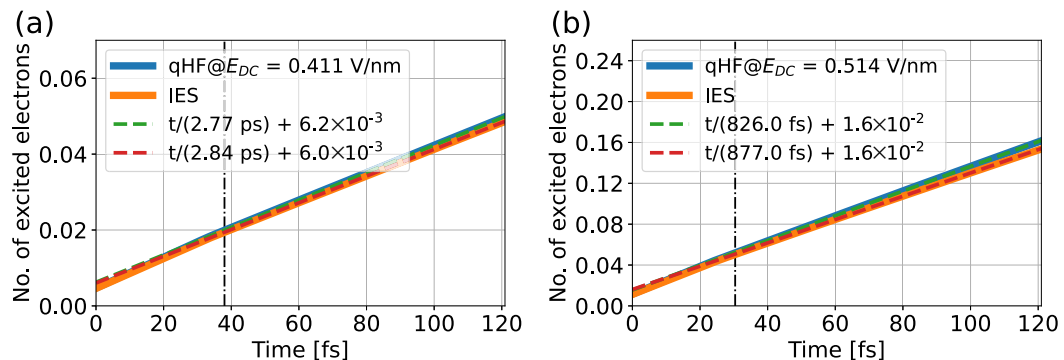

FIG. 5. Number of excited electrons as a function of time for GaAs under (a) $E_{DC} = 0.411$ V/nm and (b) $E_{DC} = 0.514$ V/nm. The T_B values of 38.0 and 30.4 fs are represented as dash-dotted vertical lines in (a) and (b), respectively.
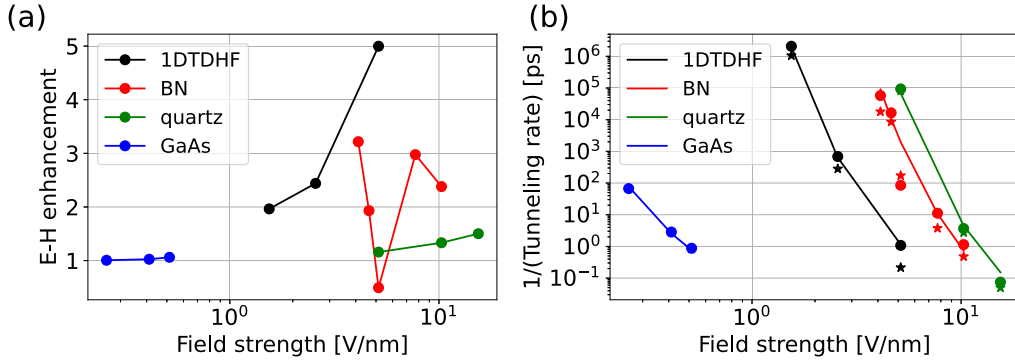
FIG. 6. (a) Enhancement factors and (b) tunneling rate inverse as a function of field strength for the 1D-TD-HF (black), BN-sheet (red), α-quartz (green), and GaAs (blue) systems. The LZ-based formula, IES, and qHF data are denoted by solid lines, solid circles, and solid stars, respectively.

eigenvalue index for each k. Note that this eigenvalue is not precisely equal to the diagonal component of the generalized Rabi frequency in Eq. (B11) because each uses a different basis to evaluate the value. Snapshots of the time-dependent eigenvalue for the 1D-TD-HF system are shown in Fig. 7. For the reference system, the IES, the eigenvalue shows an A-shifted relation $\mathcal{E}_i^k(t) = \epsilon_{i,k+A(t)}$ stemming from the velocity gauge coupling. The trivial momentum shift is subtracted to create the data in the first Brillouin zone. For the weaker-field case, 5.14 V/nm, the eigenvalue change appears symmetric for the valence and conduction bands. We also extract the reduced mass from $\mathcal{E}_i^k(t)$ by $1/\mu(t) = (\partial^2 \mathcal{E}_c^k(t)/\partial k^2)_{k=\pi/a}^{-1} - (\partial^2 \mathcal{E}_v^k(t)/\partial k^2)_{k=\pi/a}^{-1}$. The values of the renormalized gap and reduced mass are 9.375 eV and 0.0295, respectively. The renormalized electronic structure shows the asymmetric change for the stronger-field case, 10.3 V/nm: The valence band uplift is more pronounced than the conduction band drop. The values of the renormalized gap and reduced mass are 8.3 eV and 0.027. Combining the renormalized gap and effective masses into the LZ-based tunneling formula (35), we obtain 1.2 and 3.7 enhancements for 5.14 and 10.3 V/nm. These estimated values need to be higher to match the actual ionization rate enhancements, 2.44 and 4.98, in Table II. This fact suggests that renormalization of the transient dipole moment also plays a role in the enhancement. The hauling-up effect is a possible candidate for the dipole moment renormalization.

The time-dependent renormalized gap and reduced mass are also instructive for understanding the dynamics, as shown in Fig. 8. For the weaker-field case, neither the gap nor the reduced mass change over time. In contrast, the renormalized gap gradually decreases as a function of time for the stronger-field case. The renormalized reduced mass is independent of time. These facts demonstrate that the gap reduction depends on instantaneous field strength and the history of the time-dependent electric field.

VI. CONCLUSION

We developed a TD-qHF theoretical framework to investigate the role of e-h interaction in solid-state electron dynamics driven by a time-dependent electric field. The e-h interaction is included as a mean field inspired by the TD-HF method. By subtracting the trivial ground state DM in the mean-field potential, an arbitrary IES can be introduced as a reference system. The strength of the e-h interaction can be scaled up or down without any influence on the IES. This independent control of the IES and e-h interaction strength cannot be achieved by the original TD-HF method. As such, this flexible property of the TD-qHF method allows us to model a system more easily than with the TD-HF method. The equation of motion can be derived via the variational principle from an explicit energy expression; the total energy is well defined when an external field is absent.
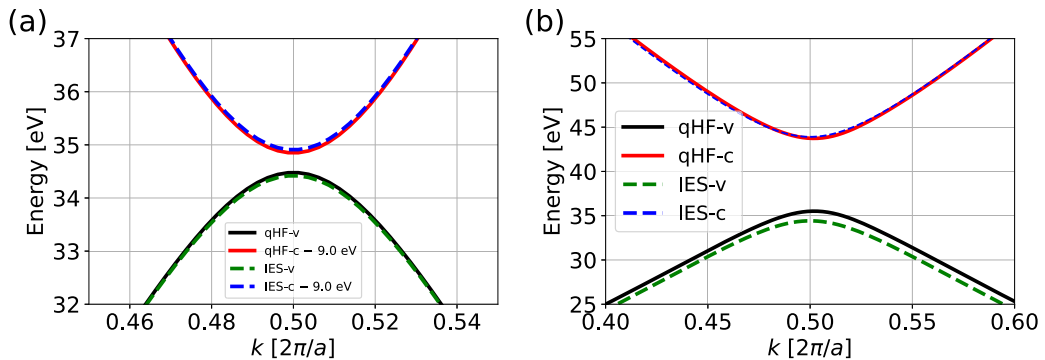

FIG. 7. Snapshots of transient electronic structures for the 1D-TD-HF system under 5.14 V/nm at $t = 60$ fs (a) and 10.3 V/nm at $t = 25$ fs (b). The conduction band energy at the top of each panel is shifted downward by 9.0 eV for visibility. Here, c, conduction band; v, valence band.
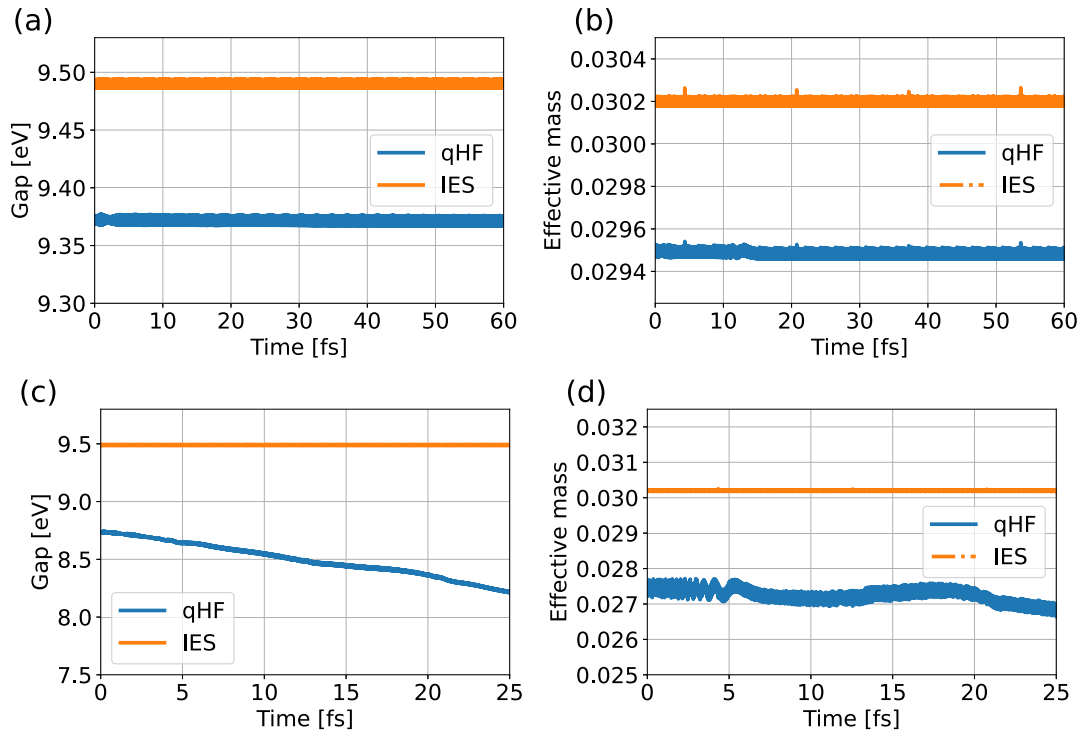
FIG. 8. Time evolution of transient gaps [(a) and (c)] and reduced masses [(b) and (d)] for 5.14 V/nm [(a) and (b)] and 10.3 V/nm [(c) and (d)].

We performed TD-qHF simulations to evaluate the e-h attraction effect in Zener tunneling. Thanks to explicit time evolution, there was no ambiguity in handling the nonperturbative response of quantum systems. A mapping to the LZ model of the IES time evolution was derived for the tunneling rate estimation. The influence of e-h interaction was investigated by comparing the TD-qHF and IES simulations using four systems imitating a 1D-TD-HF solution, a BN sheet, α-quartz, and GaAs.

Our findings showed that e-h interaction enhances the ionization rate in almost all cases. The enhancement depends on the systems as well as on the field strength. For the 1D-TD-HF, α-quartz, and GaAs systems, the enhancement showed a monotonic increase as a function of the field strength. We analyzed the transient band structure change due to e-h interaction for the 1D-TD-HF system and found that the interaction reduces the gap and the reduced mass, leading to tunneling rate promotion. However, the reductions of the gap and mass do not fully explain the enhancement. The remaining dynamical effects, such as the hauling-up effect, play an additional role in the enhancement. This theoretical framework and the results will help to clarify the mechanisms and control the dynamics of two-dimensional semiconductors (e.g., transition metal dichalcogenides) driven by a strong light field.

ACKNOWLEDGMENTS

APPENDIX A: KELDYSH PARAMETER FROM A JUMP TIME IN THE LANDAU-ZENER TRANSITION

In the analysis of the LZ model by Vitanov [33], *jump time* is introduced as a characteristic time where the diabatic population is divided by the slope of the population such that the diabatic energies are crossed. The jump time (Eq. (21) in Ref. [33]), when written as our variables, is given by

$$T^{\text{jump}} = \frac{\Delta}{\frac{1}{2}(G - G')E_{\text{DC}}} = 2\frac{\sqrt{\mu\Delta}}{E_{\text{DC}}}. \tag{A1}$$

This formula is physically interpreted as the inverse of energy associated with the field strength E_{DC} times the penetration depth $1/\sqrt{\mu\Delta}$ in the energy gap Δ between the valence and conduction bands. This equation can be obtained by taking the ratio between the diagonal and off-diagonal components of our equation of motion (32). The Keldysh parameter in Ref. [10] with an angular frequency ω is constituted by

$$\gamma_{\text{Keldysh}} = \omega \frac{T^{\text{jump}}}{2}. \tag{A2}$$

The Keldysh parameter comes from the Keldysh theory for ionization in semiconductors via a strong electric field [10].

APPENDIX B: DENSITY-MATRIX EXPRESSION OF THE TD-QHF EQUATION AND HOUSTON BASIS REPRESENTATION

We introduce an alternative expression for the TD-qHF equation with a density-matrix-based (DM-based) expression. This expression is formally elegant and simple compared with the orbital expression introduced in Sec. II. We can find an explicit connection between the SBE and the Wannier equation derived from the TD-qHF equation. Furthermore, this density-matrix-based equation can include phenomenological many-body influences such as a scattering term with relaxation time approximation. Therefore we derive here a generic theoretical framework in which the Bloch orbital is not used, since the DM composed by a Bloch orbital is not necessarily justified when we add a phenological treatment in the equation of motion beyond the qHF wave function. We only impose the BvK boundary condition, $\rho(x + N_k a, x') = \rho(x, x' + N_k a) = \rho(x, x')$, and the lattice periodicity for the simultaneous spatial translation, $\rho(x + a, x' + a) = \rho(x, x')$. Throughout this section, t in the variables is omitted except for parametrically time-dependent ones. In other words, the dynamical degrees of freedom to be determined by the equation of motion do not have explicit time coordinates in the following equations.

The total energy as a functional of the DM is given as

$$E[\rho](t) = \iint dx dx' h(x', x; t)\rho(x, x') + E_{\text{MF}}[\rho], \quad \text{(B1)}$$

$$E_{\text{MF}}[\rho] = \frac{1}{2} \iint dx dx' [\rho(x, x) - \rho_0(x, x; t)] w(x, x')[\rho(x, x) - \rho_0(x, x; t)] - \frac{1}{4} \iint dx dx' [\rho(x, x') - \rho_0(x, x'; t)]$$
$$\times w(x', x)[\rho(x', x) - \rho_0(x', x; t)], \quad \text{(B2)}$$

$$h(x, x'; t) = \delta(x - x') \left[\left(-i\frac{\partial}{\partial x'} + A(t) \right)^2 + v(x) \right], \quad \text{(B3)}$$

where spatial integration is taken over the simulation cell $0 \leqslant x, x' < N_k a$. We define a functional derivative of F with respect to the DM as

$$\left. \frac{\delta F}{\delta \rho(x, x')} \right|_{\rho} = \lim_{\epsilon \to 0} \frac{F[\rho(x, x') + \epsilon \delta \rho(x, x')] - F[\rho(x, x')]}{\epsilon}. \quad \text{(B4)}$$

Physically proper conditions for the DM are not taken into account when this functional derivative is taken. In other words, $\rho + \epsilon \delta \rho$ can be no physical DM even if ρ satisfied physically expected conditions, such as N-representability for a fermionic one-body reduced DM. We introduce the one-body Hamiltonian h_{qHF} by a functional derivative of the energy as

$$h_{\text{qHF}}(x', x; t) = \frac{\delta E(t)}{\delta \rho(x, x')} = h(x', x; t) + v_{\text{MF}}(x', x)$$

$$v_{\text{MF}}(x', x) = \left(\int dx'' w(x, x'')[\rho(x'', x'') - \rho_0(x'', x''; t)] \right)$$

$$\times \delta(x' - x) - \frac{1}{2} w(x', x)[\rho(x', x) - \rho_0(x', x; t)]. \quad \text{(B5)}$$

We can then derive the equation of motion for the DM from Eq. (12) as

$$i\frac{\partial}{\partial t}\rho(x, x') = \int dx'' [h_{\text{qHF}}(x, x''; t)\rho(x'', x') - \rho(x, x'')h_{\text{qHF}}(x'', x'; t)]. \quad \text{(B6)}$$

The total energy time derivative is given as

$$\frac{d}{dt}E = \iint dx dx' \frac{\delta E}{\delta \rho(x, x')} \frac{\partial}{\partial t}\rho(x, x') + \text{Tr}\left(\frac{\partial h(t)}{\partial t}\rho \right)$$
$$+ \left(\frac{\partial \rho_0(t)}{\partial t} \text{ related terms} \right)$$
$$= -i\text{Tr}(h_{\text{qHF}}h_{\text{qHF}}\rho) + i\text{Tr}(h_{\text{qHF}}\rho h_{\text{qHF}})$$
$$+ \frac{dA}{dt}\text{Tr}\left(\left[-i\frac{\partial}{\partial x} + A(t) \right]\rho \right) - \frac{1}{2}\text{Tr}\left(\left[\frac{\partial \rho_0(t)}{\partial t}w \right]\rho \right), \quad \text{(B7)}$$

where the trace is achieved by the spatial integration over the simulation cell. To obtain the last line, we use $\partial \rho_0(t)/\partial t = i\dot{A}[x, \rho_0(t)]$ and $\text{Tr}([x, \rho_0(t)]\rho_0(t)) = 0$. The first and second terms in the final equation cancel each other out by the cyclic exchange in the trace. Therefore the total energy is kept constant when the A field is a constant in time.

We derive an expression to solve (B6) in the Houston basis [39] without a time-dependent phase factor as

$$\rho(x, x') = \frac{2}{N_k} \sum_{\alpha\beta k} e^{ikx} v_{\alpha,k+A(t)}(x) \rho_{\alpha\beta}^k v_{\beta,k+A(t)}^* e^{-ikx'}, \quad \text{(B8)}$$

where justification of the k-dependent decompositions is presented in Appendix C. The reason for phase factor omission here is to resemble the SBE for the TD-qHF method. Matrix elements for a spatially nonlocal function $O(x, x')$ of the basis are defined as

$$O_{\alpha\beta}^k(t) = \frac{1}{N_k} \int_0^{N_k a} dx \int_0^{N_k a} dx' \, e^{-ikx} v_{\alpha,k+A(t)}^*(x) O(x, x'; t)$$
$$\times e^{+ikx'} v_{\beta,k+A(t)}(x'). \quad \text{(B9)}$$

Substituting Eq. (B8) into Eq. (B6), we obtain the equation of motion for $\rho_{\alpha\beta}$ as

$$i\frac{d}{dt}\rho_{\alpha\beta}^k = [\epsilon_{\alpha k+A(t)} - \epsilon_{\beta k+A(t)}]\rho_{\alpha\beta}^k$$
$$+ \sum_\gamma \Omega_{\alpha\gamma}^k(t)\rho_{\gamma\beta}^k - \sum_\gamma \rho_{\alpha\gamma}^k \Omega_{\gamma\beta}^k(t), \quad \text{(B10)}$$

$$\Omega_{\alpha\beta}^k(t) = -\dot{A}(t)\mathcal{X}_{\alpha\beta}(k + A(t)) + v_{\text{MF},\alpha\beta}^k,$$

$$\mathcal{X}_{\alpha\beta}(k) = \left\langle v_{\alpha k} \left| \frac{\partial v_{\beta k}}{\partial k} \right. \right\rangle = \int_0^a dx v_{\alpha k}^* \frac{\partial v_{\beta k}(x)}{\partial k}, \quad \text{(B11)}$$

where $\langle v_{\alpha k} | \frac{\partial v_{\beta k}}{\partial k} \rangle = -\langle \frac{\partial v_{\alpha k}}{\partial k} | v_{\beta k} \rangle$ is used. $\Omega_{\alpha\beta}^k$ is the generalized Rabi frequency for the TD-qHF method. Explicit construction of the MF-term matrix element for $\varrho = \rho, \rho_0$

is given as

$$
v_{\text{MF},\alpha\beta}^{k}[\varrho] = \sum_{H} w^{q=0}(H)\eta(H)\langle v_{\alpha k+A(t)}|e^{iHx}|v_{\beta k+A(t)}\rangle \left(\sum_{k'\gamma\delta} \varrho_{\gamma\delta}^{k'}\langle v_{\gamma k+A(t)}|e^{-iHx}|v_{\delta k+A(t)}\rangle \right)
$$
$$
- \frac{1}{2}\sum_{qH\gamma\delta} w^{q}(H)\varrho_{\gamma\delta}^{k-q}\langle v_{\alpha,k+A(t)}|e^{iHx}|v_{\gamma,k-q+A(t)}(t)\rangle\langle v_{\delta,k-q+A(t)}(t)|e^{-iHx}|v_{\beta,k+A(t)}\rangle. \tag{B12}
$$

We introduce two approximations: first, that the Coulombic interaction has only a long-range part,

$$
w^{q}(H) = \bar{w}^{q}\delta_{H,0}, \tag{B13}
$$

and second, that the LPP labeled by the eigenfunction is the same for all crystal momenta,

$$
\langle v_{\alpha k}|v_{\alpha k'}\rangle = 1. \tag{B14}
$$

Within the approximation, we obtain the mean-field part as

$$
v_{\text{SBE},\alpha\beta}^{k}[\rho - \rho_0] = -\frac{1}{2}\sum_{q} \bar{w}^{q}\big\{\rho_{\alpha\beta}^{k-q}(t) - \rho_{0,\alpha\beta}^{k-q}\big\}. \tag{B15}
$$

The equation of motion with the approximation is

$$
i\frac{d}{dt}\rho_{\alpha\beta}^{k} = [\epsilon_{\alpha k+A(t)} - \epsilon_{\beta k+A(t)}]\rho_{\alpha\beta}^{k}
$$
$$
+ \sum_{\gamma} \Omega_{\text{SBE},\alpha\gamma}^{k}(t)\rho_{\gamma\beta}^{k} - \sum_{\gamma} \rho_{\alpha\gamma}^{k}\Omega_{\text{SBE},\gamma\beta}^{k}(t), \tag{B16}
$$

$$
\Omega_{\text{SBE},\alpha\beta}^{k}(t) = -\dot{A}(t)\mathcal{X}_{\alpha\beta}(k+A(t)) + v_{\text{SBE},\alpha\beta}^{k}. \tag{B17}
$$

We restrict ourselves to a two-band system achieved by $(\alpha,\beta) = (v,v),(v,c),(c,v),(c,c)$. The equations of motion are given as

$$
i\frac{d}{dt}\rho_{vc}^{k} = [e_{ck}(t) - e_{vk}(t)]\rho_{vc}^{k}
$$
$$
+ \big[\rho_{vv}^{k}(t) - \rho_{cc}^{k}(t)\big]\Omega_{\text{SBE},vc}^{k}[\rho],
$$
$$
e_{ck}(t) = \epsilon_{ck+A(t)} - \frac{1}{2}\sum_{q} \bar{w}^{q}\rho_{cc}^{k-q},
$$
$$
e_{vk}(t) = \epsilon_{vk+A(t)} - \frac{1}{2}\sum_{q} \bar{w}^{q}\big(\rho_{vv}^{k-q} - 2\big),
$$
$$
i\frac{d}{dt}\rho_{vv}^{k} = \rho_{vc}^{k}\Omega_{\text{SBE},cv}^{k}[\rho] - \Omega_{\text{SBE},vc}^{k}[\rho]\rho_{cv}^{k},
$$
$$
i\frac{d}{dt}\rho_{cc}^{k}(t) = \rho_{cv}^{k}\Omega_{\text{SBE},vc}^{k}[\rho] - \Omega_{\text{SBE},cv}^{k}[\rho]\rho_{vc}^{k}. \tag{B18}
$$

These are nothing but SBEs, while minor differences are as follows. In the original SBE construction, a bare electronic structure is given as a reference system, and it is renormalized by the electron-hole interaction even without an external field. In our TD-qHF formulation, an already renormalized electronic structure is introduced by subtracting the initial density matrix ρ_0. In front of the electron-hole attraction, the $1/2$ factor appears because of the exchange interaction for the spin-restricted electron system within the qHF method. The intraband motion in the eigenvalue $\epsilon_{vk+A(t)}$ comes from the velocity gauge ansatz for the equation of motion. In

the velocity gauge, we determine that the counterpart to the dipole operator matrix element is $\mathcal{X}_{\alpha\beta}$ by taking into account $\dot{A} = -E(t)$.

Within the two-band SBE, the gap renormalization of the relative energy between conduction and valence bands is calculated as

$$
e_{ck}(t) - e_{vk}(t) = \epsilon_{ck+A(t)} - \epsilon_{vk+A(t)} - \sum_{q} \bar{w}^{q}\rho_{cc}^{k-q}, \tag{B19}
$$

where the conservation rule $\rho_{cc}^{k-q}(t) + \rho_{vv}^{k-q}(t) = 2$ is used. Thus the band gap shrinks by increasing the conduction band population.

For the Wannier equation in our framework, we apply the linear perturbation theory for Eq. (B18) by $\rho(t) \simeq \rho_0 + \delta\rho(t)$ and neglect the momentum shift due to the A field. The equation for $\delta\rho$ is

$$
i\frac{d}{dt}\delta\rho_{vc}^{k} = [\epsilon_{ck} - \epsilon_{vk}]\delta\rho_{vc}^{k} - \sum_{q} \bar{w}^{q}\delta\rho_{vc}^{k-q} + 2\mathcal{X}_{vc}^{k}E(t). \tag{B20}
$$

By taking the correspondence $k \to \hat{k} = -i\partial/\partial X$, we obtain the real-space counterpart via Fourier transformation:

$$
i\frac{d}{dt}W_{vc}(X,t) = [\epsilon_c(\hat{k}) - \epsilon_v(\hat{k}) - \bar{w}(X)]W_{vc}(X,t)
$$
$$
+ 2\mathcal{X}_{vc}(X)E(t). \tag{B21}
$$

When the eigenvalue difference is approximated as $\epsilon_{ck} - \epsilon_{vk} \simeq \Delta + \frac{k^2}{2\mu}$, an eigenvalue equation for the homogeneous part of (B21) is

$$
\left[\Delta - \frac{1}{2\mu}\frac{\partial^2}{\partial X^2} - \bar{w}(X)\right]W_{vc}(X) = E_{\text{op}}W_{vc}(X). \tag{B22}
$$

This is the Wannier equation.

If we use the Houston basis with the trivial phase factor, as

$$
\rho^{k}(x,x') = \sum_{\alpha\beta} e^{-i\int_0^t dt'\epsilon_{\alpha k+A(t')}}v_{\alpha,k+A(t)}\tilde{\rho}_{\alpha\beta}^{k}v_{\beta,k+A(t)}^{*}e^{+i\int_0^t dt'\epsilon_{\beta k+A(t')}}, \tag{B23}
$$

where $(v_{\alpha,k},\epsilon_{\alpha,k})$ is the eigenpair of the field-free Hamiltonian without an MF part, $\int dx' h(x,x';t=0)e^{ikx'}v_{\alpha,k}(x') = \epsilon_{\alpha k}e^{ikx}v_{\alpha,k}(x)$. The equation of motion for $\rho_{\alpha\beta}^{k}$ reads

$$
i\frac{d}{dt}\tilde{\rho}_{\alpha\beta}^{k} = \sum_{\gamma} e^{+i\int_0^t (\epsilon_{\alpha k+A(t')} - \epsilon_{\gamma k+A(t')})}\Omega_{\alpha\gamma}^{k}(t)\tilde{\rho}_{\gamma\beta}^{k}
$$
$$
- \sum_{\gamma} e^{-i\int_0^t (\epsilon_{\beta k+A(t')} - \epsilon_{\gamma k+A(t')})}\tilde{\rho}_{\alpha\gamma}^{k}\Omega_{\gamma\beta}^{k}(t), \tag{B24}
$$

where the definition of the generalized Rabi frequency $\Omega_{\gamma\beta}^k(t)$ is the same as (B11). This equation of motion is simply another expression of Eq. (9) in Ref. [27]. $\tilde{\rho}_{\alpha\beta}$ varies slowly compared with the energy difference $\epsilon_{\beta k} - \epsilon_{\alpha k}$ because of the phase factor inclusion in the Houston basis representation. The term that has $-\dot{A}(t)\mathcal{X}$ is expected to be off-resonant because $\langle v_{\alpha k}|\partial v_{\gamma k}/\partial k\rangle_{k+A(t)}$ has only slowly varying components. The resonant oscillation component only comes from $v_{\text{MF},\alpha\gamma}^k \simeq e^{-i\int_0^t (\epsilon_{\alpha k+A(t')} - \epsilon_{\gamma k+A(t')})}$ as pointed out in Ref. [27].

APPENDIX C: NONLOCAL FUNCTION WITH LATTICE PERIODICITY

Generally, a function with two spatial coordinates $f(x, x')$ requires two wave numbers for the Fourier transformation. Here, we prove that a function that satisfies $f(x + N_k a, x') = f(x, x' + N_k a) = f(x, x')$, $f(x + a, x' + a) = f(x, x')$ has a particular form for the Fourier transformation that has single crystal momentum and two reciprocal lattice coordinates. We prove this form to validate the decomposition form (B8).

Consider a function $f(x, x')$ within the BvK boundary condition $f(x + N_k a, x') = f(x, x' + N_k a) = f(x, x')$. We further assume a lattice periodicity for simultaneous spatial variable translation as

$$f(x + a, x' + a) = f(x, x'). \tag{C1}$$

This condition appears in the one-body reduced DM and one-body Green's function in typical many-body problems for perfect crystals.

This function can be expanded as

$$f(x, x') = \sum_k e^{ikx} f^k(x, x') e^{-ikx},$$
$$f^k(x + a, x') = f^k(x, x' + a) = f^k(x, x'), \tag{C2}$$

where k is the discretized wave number $k = 0, 2\pi/(N_k a), \ldots, 2\pi/(N_k a)(N_k - 1)$, as in the orbital case.

This single k expansion is proved by starting from a general Fourier expansion:

$$f(x, x') = \sum_{kk'GG'} e^{+i(k+G)x} \tilde{f}^{k,k'}(G, G') e^{-i(k'+G')x'},$$
$$\tilde{f}^{k,k'}(G, G') = \frac{1}{(N_k a)^2} \iint dx\,dx'\, e^{-i(k+G)x} f(x, x') e^{+i(k'+G')x'}, \tag{C3}$$

where k, k' are discretized Brillouin zone indices and G, G' varies the reciprocal lattices. Using the simultaneous translation for this formula, we obtain

$$f(x + a, x' + a) = \sum_{kk'GG'} e^{+i(k-k')a} e^{+i(k+G)x} \tilde{f}^{k,k'}(G, G')$$
$$\times e^{-i(k'+G')x'}. \tag{C4}$$

Since all components are the same, we obtain $e^{+i(k-k')a} = 1$ for an arbitrary (k, k') pair. This means that k' is equal to k, namely, a single k index is sufficient for $\tilde{f}^{k,k'}(G, G) \to f^k(G, G')$. Thus the proper expansion is given as

$$f(x, x') = \sum_{kGG'} e^{+i(k+G)x} f^k(G, G') e^{-i(k+G')x'},$$
$$f^k(G, G') = \frac{1}{(N_k a)^2} \iint dx\,dx'\, e^{-i(k+G)x} f(x, x') e^{+i(k+G')x'}. \tag{C5}$$

By taking the partial sum over the reciprocal lattices, we have the following formula:

$$f(x, x') = \sum_k e^{+ikx} f^k(x, x'') e^{-ikx'},$$
$$f^k(x, x') = \sum_{GG'} e^{+iGx} f^k(G, G') e^{-iG'x'}. \tag{C6}$$

$f^k(x + a, x') = f^k(x, x' + a) = f^k(x, x')$ can be confirmed from this formula.

Note that we do not impose any condition on f except for the BvK boundary condition and the simultaneous lattice translation symmetry. We can derive a more specific formula with a more explicit form for f. The one-body reduced DM composed by a Slater determinant with Bloch orbitals, for example, has the following factorized shape:

$$\rho(x, x') = \frac{2}{N_k} \sum_{ik} e^{+ikx} u_{ik}(x) u_{ik}^*(x') e^{-ikx'}. \tag{C7}$$

The Fourier component of the k-dependent DM also has a factorial shape:

$$\rho^k(G, G') = \frac{2}{N_k} \sum_i u_{ik}(G) u_{ik}^*(G'). \tag{C8}$$

[1] F. Rossi and T. Kuhn, Theory of ultrafast phenomena in photoexcited semiconductors, Rev. Mod. Phys. **74**, 895 (2002).

[2] S. Ghimire, G. Ndabashimiye, A. D. DiChiara, E. Sistrunk, M. I. Stockman, P. Agostini, L. F. DiMauro, and D. A. Reis, Strong-field and attosecond physics in solids, J. Phys. B: At. Mol. Opt. Phys. **47**, 204030 (2014).

[3] S. Y. Kruchinin, F. Krausz, and V. S. Yakovlev, Colloquium: Strong-field phenomena in periodic systems, Rev. Mod. Phys. **90**, 021002 (2018).

[4] S. Ghimire and D. A. Reis, High-harmonic generation from solids, Nat. Phys. **15**, 10 (2019).

[5] L. Yue and M. B. Gaarde, Introduction to theory of high-harmonic generation in solids: Tutorial, J. Opt. Soc. Am. B **39**, 535 (2022).

[6] B. N. Chichkov, C. Momma, S. Nolte, F. von Alvensleben, and A. Tünnermann, Femtosecond, picosecond and nanosecond laser ablation of solids, Appl. Phys. A **63**, 109 (1996).

[7] P. Balling and J. Schou, Femtosecond-laser ablation dynamics of dielectrics: Basics and applications for thin films, Rep. Prog. Phys. **76**, 036502 (2013).

[8] K. Sugioka and Y. Cheng, Femtosecond laser three-dimensional micro- and nanofabrication, Appl. Phys. Rev. **1**, 041303 (2014).

[9] P. B. Corkum, Plasma perspective on strong field multiphoton ionization, Phys. Rev. Lett. **71**, 1994 (1993).

[10] L. V. Keldysh, Ionization in the field of a strong electromagnetic wave, Sov. Phys. JETP **20**, 1307 (1965).

[11] T. Mueller and E. Malic, Exciton physics and device application of two-dimensional transition metal dichalcogenide semiconductors, npj 2D Mater. Appl. **2**, 29 (2018).

[12] G. Onida, L. Reining, and A. Rubio, Electronic excitations: Density-functional versus many-body Green's-function approaches, Rev. Mod. Phys. **74**, 601 (2002).

[13] X. Leng, F. Jin, M. Wei, and Y. Ma, GW method and Bethe-Salpeter equation for calculating electronic excitations, WIREs Comput. Mol. Sci. **6**, 532 (2016).

[14] L. Reining, The GW approximation: Content, successes and limitations, WIREs Comput. Mol. Sci. **8**, e1344 (2018).

[15] C. Zener, A theory of the electrical breakdown of solid dielectrics, Proc. R. Soc. London, Ser. A **145**, 523 (1934).

[16] A. Di Carlo, P. Vogl, and W. Pötz, Theory of Zener tunneling and Wannier-Stark states in semiconductors, Phys. Rev. B **50**, 8358 (1994).

[17] A. Sibille, J. F. Palmier, and F. Laruelle, Zener interminiband resonant breakdown in superlattices, Phys. Rev. Lett. **80**, 4506 (1998).

[18] B. Rosam, D. Meinhold, F. Löser, V. G. Lyssenko, S. Glutsch, F. Bechstedt, F. Rossi, K. Köhler, and K. Leo, Field-induced delocalization and Zener breakdown in semiconductor superlattices, Phys. Rev. Lett. **86**, 1307 (2001).

[19] C. F. Bharucha, K. W. Madison, P. R. Morrow, S. R. Wilkinson, B. Sundaram, and M. G. Raizen, Observation of atomic tunneling from an accelerating optical potential, Phys. Rev. A **55**, R857(R) (1997).

[20] M. Glück, A. R. Kolovsky, and H. J. Korsch, Lifetime of Wannier-Stark states, Phys. Rev. Lett. **83**, 891 (1999).

[21] M. Holthaus, Bloch oscillations and Zener breakdown in an optical lattice, J. Opt. B: Quantum Semiclass. Opt. **2**, 589 (2000).

[22] R. Takahashi and N. Sugimoto, Landau-Zener tunneling problem for Bloch states, Phys. Rev. B **95**, 224302 (2017).

[23] B. Wu and Q. Niu, Nonlinear Landau-Zener tunneling, Phys. Rev. A **61**, 023402 (2000).

[24] H. Haug and S. W. Koch, *Quantum Theory of the Optical and Electronic Properties of Semiconductors*, 5th ed. (World Scientific, Singapore, 2009).

[25] M. Lindberg and S. W. Koch, Effective Bloch equations for semiconductors, Phys. Rev. B **38**, 3342 (1988).

[26] M. Garg, M. Zhan, T. T. Luu, H. Lakhotia, T. Klostermann, A. Guggenmos, and E. Goulielmakis, Multi-petahertz electronic metrology, Nature (London) **538**, 359 (2016).

[27] T. Ikemachi, Y. Shinohara, T. Sato, J. Yumoto, M. Kuwata-Gonokami, and K. L. Ishikawa, Time-dependent Hartree-Fock study of electron-hole interaction effects on high-order harmonic generation from periodic crystals, Phys. Rev. A **98**, 023415 (2018).

[28] J. R. Williams, N. Tancogne-Dejean, and C. A. Ullrich, Time-resolved exciton wave functions from time-dependent density-functional theory, J. Chem. Theory Comput. **17**, 1795 (2021).

[29] J. Li, X. Zhang, S. Fu, Y. Feng, B. Hu, and H. Du, Phase invariance of the semiconductor Bloch equations, Phys. Rev. A **100**, 043404 (2019).

[30] S. Jiang, C. Yu, J. Chen, Y. Huang, R. Lu, and C. D. Lin, Smooth periodic gauge satisfying crystal symmetry and periodicity to study high-harmonic generation in solids, Phys. Rev. B **102**, 155201 (2020).

[31] C. Kittel, *Introduction to Solid State Physics*, 8th ed. (Wiley, New York, 2004).

[32] S. A. Sato, Y. Taniguchi, Y. Shinohara, and K. Yabana, Nonlinear electronic excitations in crystalline solids using meta-generalized gradient approximation and hybrid functional in time-dependent density functional theory, J. Chem. Phys. **143**, 224116 (2015).

[33] N. V. Vitanov, Transition times in the Landau-Zener model, Phys. Rev. A **59**, 988 (1999).

[34] S. Glutsch, Nonresonant and resonant Zener tunneling, Phys. Rev. B **69**, 235317 (2004).

[35] T. Otobe, M. Yamagiwa, J.-I. Iwata, K. Yabana, T. Nakatsukasa, and G. F. Bertsch, First-principles electron dynamics simulation for optical breakdown of dielectrics under an intense laser field, Phys. Rev. B **77**, 165104 (2008).

[36] F. Ferreira, A. J. Chaves, N. M. R. Peres, and R. M. Ribeiro, Excitons in hexagonal boron nitride single-layer: A new platform for polaritonics in the ultraviolet, J. Opt. Soc. Am. B **36**, 674 (2019).

[37] S. S. Nekrashevich and V. A. Gritsenko, Electronic structure of silicon dioxide (a review), Phys. Solid State **56**, 207 (2014).

[38] A. M. Cohen and G. E. Marques, Electronic structure of zinc-blende-structure semiconductor heterostructures, Phys. Rev. B **41**, 10608 (1990).

[39] W. V. Houston, Acceleration of electrons in a crystal lattice, Phys. Rev. **57**, 184 (1940).